

Study on accelerator neutrino detection at a spallation source ^{*}

Huang Ming-Yang^{1,2;1)}¹ China Spallation Neutron Source (CSNS), Institute of High Energy Physics (IHEP), Chinese Academy of Sciences (CAS), Dongguan 523803, China² Dongguan Institute of Neutron Science (DINS), Dongguan 523808, China**Abstract:**

In this paper, we study the detection of accelerator neutrinos at the China Spallation Neutron Source (CSNS). By using the code FLUKA, the processes of accelerator neutrinos production during the proton beam hitting on the tungsten target are simulated, and the yield efficiency, numerical flux, average energy of different flavor neutrinos are obtained. Furthermore, the detection of accelerator neutrinos through two reaction channels, the neutrino-electron reactions and neutrino-carbon reactions, is studied, and the event numbers of different flavor neutrinos are calculated.

Key words: spallation source, accelerator neutrinos, numerical flux, event number**PACS:** 14.60.Pq, 25.40.Sc, 29.25.-t

1 Introduction

Over the last several decades, many spallation neutron sources (the Los Alamos Meson Physics Facility (LAMPF), the Spallation Neutron Source at Rutherford Appleton Laboratory (ISIS) [1], the Japan Accelerator Research Complex (J-PARC) [2], the Spallation Neutron Source at Oak Ridge National Laboratory (SNS) [3] et al.) have started operation. In recent years, some new spallation neutron sources (the China Spallation Neutron Source (CSNS) [4], the European Spallation Neutron Source (ESS) [5] et al.) are under construction.

These spallation neutron sources are designed to provide multidisciplinary platforms for scientific research and applications for national institutions, universities, and industries [6, 7]. Application fields include basic energy sciences, particle physics, and nuclear sciences. Table 1 shows the main technical parameters for some spallation neutron sources at GeV energy range in the world. For J-PARC, the technical parameters shown in the table belong to the Rapid Cycling Synchrotron (RCS).

Table 1. Main technical parameters for some spallation neutron sources at GeV energy range (ppp means protons per pulse).

	Extraction energy (GeV)	Extraction power (MW)	Repetition rate (Hz)	Average beam Current (mA)	Intensity (10^{13} ppp)	Target
LAMPF [8]	0.8	0.056	120	1	2.3	Various
ISIS [9, 10]	0.8	0.16	50	0.2	2.5	Water cooled /Tantalum
J-PARC [11, 12]	3.0	1.0	25	0.333	8.3	Mercury
SNS [13, 14]	1.0	1.4	60	1.6	16	Mercury
CSNS-I(II) [15, 16]	1.6	0.1(0.5)	25	0.063(0.315)	1.56(7.8)	Tungsten
ESS [17]	2.0	5.0	14	62.5	110	Tungsten

CSNS consists of an 80 MeV proton linac, a 1.6 GeV RCS, a solid tungsten target station, and instruments for spallation neutron applications [18]. The accelerator operates at 25 HZ repetition rate with an initial design beam power of 100 kW and is upgradeable to 500 kW. As the exclusive spallation neutron source in developing countries, CSNS will be among the top four of such facilities in the world until completion. Table 2 shows the

main design parameters for CSNS-I and CSNS-II [15, 16].

A large number of accelerator neutrinos can be produced by the decays of pions and muons at the beam stops of high intensity proton accelerators. Neutrino beams at proton accelerators have been served as laboratories for better understanding of the neutrino property, and the neutrinos have been harnessed as a probe to better understand the weak interaction force [19]. Dur-

* Supported by National Natural Science Foundation of China (Nos.11205185 and 11175020)

1) E-mail: huangmy@ihep.ac.cn

ing the last several decades, many neutrino experiments based on spallation neutron sources [20] (the Liquid Scintillator Neutrino Detector (LSND) [8] at LAMPF, the Karlsruhe Rutherford Medium Energy Neutrino experiment (KARMEN) [21, 22] at ISIS, the Tokai-to-Kamioka experiment (T2K) [23] at J-PARC et al.). For CSNS, a large number of accelerator neutrinos can be produced during the high intensity proton beam hitting on the tungsten target. By using a neutrino detector similar to MiniBooNE [24], a lot of accelerator neutrinos can be detected. Therefore, some information about neutrino property and neutrino mixing parameters may be obtained.

Table 2. Main design parameters of CSNS.

Parameter/unit	CSNS-I	CSNS-II
Beam power on target/MW	0.1	0.5
Linac energy/GeV	0.08	0.25
Beam energy on target/GeV	1.6	1.6
Average beam current/ μA	62.5	315
Pulse repetition rate/Hz	25	25
Ion type, source linac	H^-	H^-
Protons per pulse/ 10^{13}	1.56	7.8
Target material	Tungsten	Tungsten
Target number	1	1
Target size/mm ³	$50 \times 150 \times 400$	$50 \times 150 \times 400$
Beam section/mm ²	40×100	40×100

2 Accelerator Neutrino Beam

The idea of accelerator neutrino beam was initiated independently by Schwartz and Pontecorvo, and the experiment of which, firstly, was carried out by Lederman, Schwartz, Steinberger with other collaborators [19, 25]. Low energy neutrino beams can be produced by the decay of π , μ mesons at rest, which are generated during the proton beam hitting on the target. In a beam dump experiment, the target for the primary proton beam, where the neutrino parents are produced, is the medium for absorbing or stopping the hadrons. Therefore, no drift space is provided for hadrons to decay in. High intensity, low energy proton accelerators ($p_{beam} \sim 1 \text{ GeV}/c$) such as spallation neutron sources are commonly used [26, 27]. The decays of π , μ mesons at rest gives an nearly equal number of ν_μ , $\bar{\nu}_\mu$, and ν_e with a characteristic low energy spectrum. The two recent experiments at a beam dump, LSND and KARMEN, have given controversial results on neutrino oscillations which were solved by the MiniBooNE experiment [28, 29].

The dominant decay scheme that produces neutrinos from a stopped pion source is [30]

$$\pi^+ \longrightarrow \mu^+ + \nu_\mu, \quad \tau_\pi = 26ns, \quad (1)$$

followed by

$$\mu^+ \longrightarrow e^+ + \bar{\nu}_\mu + \nu_e, \quad \tau_\mu = 2.2\mu s, \quad (2)$$

where τ_π (τ_μ) is the life time of π^+ (μ^+).

The bulk of the π^- 's produced are strong absorbed by the target before they are able to decay, and most of the μ^- 's which are produced from π^- decay are captured from the atomic orbit, a process which does not give $\bar{\nu}_e$. Therefore, the yield efficiency of $\bar{\nu}_e$ is a factor of 10^{-3} to 10^{-4} lower than that of the other neutrino species, and it will be neglected in the following discussions.

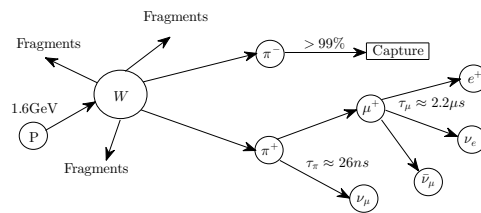


Fig. 1. The accelerator neutrino production mechanism at CSNS.

The CSNS beam stop will provide a copious flux of decay at rest neutrinos, primarily from π^+ and μ^+ decays. Fig. 1 shows the neutrino production in the CSNS tungsten beam stop. By using the code FLUKA [31] and the main design parameters of CSNS given in Table 2, the processes that the 1.6 GeV proton beam hitting on the tungsten target were simulated. The simulation results show that different flavor neutrinos (ν_e , ν_μ , $\bar{\nu}_\mu$) have the same yield efficiency which is about 0.17 per proton. In Table 3, the event numbers per year of accelerator neutrinos produced at CSNS are given. We find that three kinds of accelerator neutrinos have the same yield event number per year which is 0.21×10^{22} for CSNS-I and 1.05×10^{22} for CSNS-II. Since it will rise ultimately to 500 KW in the future with more neutrinos produced, the main parameters for CSNS-II will be considered mainly in the following discussions.

Table 3. Event numbers per year of accelerator neutrinos produced at CSNS.

	CSNS-I	CSNS-II
Proton number per year/ 10^{22}	1.23	6.15
ν_e number per year/ 10^{22}	0.21	1.05
ν_μ number per year/ 10^{22}	0.21	1.05
$\bar{\nu}_\mu$ number per year/ 10^{22}	0.21	1.05

The numerical flux ϕ of each particle (π^+ , μ^+ , ν_e , ν_μ , $\bar{\nu}_\mu$) can be given by [32]

$$\phi(L) = \frac{\varphi(\text{num/year})}{4\pi L^2(\text{cm}^2)}, \quad (3)$$

where L is the distance between the center of spallation target and the center of neutrino detector, and φ is the yield event number per year. By using the code FLUKA, the yield efficiency of different particles can be obtained, and then the numerical flux can be calculated by using Eq. (3). Fig. 2 shows that:

- (i) The numerical fluxes of various particles all decrease with the distance L ;
- (ii) ν_e and $\bar{\nu}_\mu$ have the same numerical flux;
- (iii) The numerical flux of ν_μ is larger than that of ν_e and $\bar{\nu}_\mu$;
- (iv) The numerical flux of π^+ decreases very quickly with the distance L .

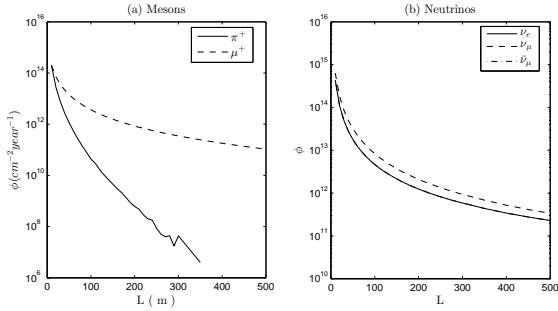


Fig. 2. The numerical flux of each particle (π^+ , μ^+ , ν_e , ν_μ , $\bar{\nu}_\mu$) as a function of the distance L . (a) π^+ and μ^+ ; (b) ν_e , ν_μ , and $\bar{\nu}_\mu$.

During the simulation of neutrino production, the average energy of different flavor neutrinos was also obtained. It can be found that the average energy of ν_e is much smaller than that of ν_μ and $\bar{\nu}_\mu$.

While considering the oscillations between ν_e , ν_μ , and ν_τ , the oscillation probabilities, neglecting matter effects, for accelerator neutrinos in the three flavor mixing scheme while $\Delta m_{12}^2 = 7.5 \times 10^{-5} \text{ eV}^2$ and $L/E \simeq 1$ (i.e. $\sin^2(\Delta m_{12}^2 \cdot L/4E) \simeq 0$) are [33]

$$\begin{aligned} P(\nu_e \rightarrow \nu_\mu) &\simeq \sin^2 \theta_{23} \sin^2 2\theta_{13} \sin^2(\Delta m^2 \cdot L/4E_\nu), \\ P(\nu_e \rightarrow \nu_\tau) &\simeq \cos^2 \theta_{23} \sin^2 2\theta_{13} \sin^2(\Delta m^2 \cdot L/4E_\nu), \\ P(\nu_\mu \rightarrow \nu_\tau) &\simeq \cos^4 \theta_{13} \sin^2 2\theta_{23} \sin^2(\Delta m^2 \cdot L/4E_\nu), \end{aligned} \quad (4)$$

where $\Delta m_{23}^2 = 2.4 \times 10^{-3} \text{ eV}^2$, $\sin^2 \theta_{23} = 0.446$, $\sin^2 \theta_{13} = 0.0237$ [34], E_ν is the neutrino energy, and L is the baseline (the distance of the neutrino source from the detector). Suppose the baseline $L = 60 \text{ m}$, it can be calculated that $P(\nu_e \rightarrow \nu_\mu) \simeq 1.27 \times 10^{-6}$, $P(\nu_e \rightarrow \nu_\tau) \simeq 1.57 \times 10^{-6}$, and $P(\nu_\mu \rightarrow \nu_\tau) \simeq 1.26 \times 10^{-5}$. Therefore, the oscillations between ν_e , ν_μ , and ν_τ will be out of discussions in below in this paper.

In the next section, the processes of accelerator neutrino detection will be studied, and the neutrino event numbers observed through various reaction channels will be calculated.

3 Detection of accelerator neutrinos

In the above section, the production of accelerator neutrinos has been studied, and the yield efficiency, numerical flux, average energy of different flavor neutrinos were obtained. In this section, the detection of accelerator neutrinos will be studied.

The event numbers per year \tilde{N}_i of accelerator neutrinos observed through various reaction channels i can be calculated by [35]

$$\tilde{N}_i = \phi(\nu/\text{year}/\text{cm}^2) \cdot \sigma_i(\text{cm}^2) \cdot N_T, \quad (5)$$

where ϕ is the neutrino numerical flux given in Eq. (3), σ_i is the cross section of the given neutrino reaction, and N_T is the target number.

For the accelerator neutrino detection at CSNS, a detector similar to MiniBooNE is adopted in the following discussions [24]. It consists of a 6.1 m radius spherical tank filled with approximately 803 tons of mineral oil (CH_2). Then the total event numbers of target protons, electrons, and ^{12}C are

$$\begin{aligned} N_T^{(p)} &= 6.90 \times 10^{31}, & N_T^{(e)} &= 2.76 \times 10^{32}, \\ N_T^{(C)} &= 3.45 \times 10^{31}. \end{aligned}$$

By using the above detector, two reaction channels were used to detect accelerator neutrinos (ν_e , ν_μ , $\bar{\nu}_\mu$) at CSNS:

(1) Neutrino-electron reactions

$$\begin{aligned} \nu_e + e^- &\rightarrow \nu_e + e^- \quad (\text{CC and NC}), \\ \nu_\mu + e^- &\rightarrow \nu_\mu + e^- \quad (\text{NC}), \\ \bar{\nu}_\mu + e^- &\rightarrow \bar{\nu}_\mu + e^- \quad (\text{NC}), \end{aligned}$$

where CC and NC stand respectively for the changed current and neutral current interactions, producing recoil electrons with energy from zero up to the kinematics maximum.

(2) Neutrino-carbon reactions

For the neutrinos and ^{12}C system, there are one charged-current and three neutral-current reactions:

Charged-current capture

$$\begin{aligned} \nu_e + ^{12}\text{C} &\rightarrow ^{12}\text{N} + e^-, & E_{th} &= 17.34 \text{ MeV}, \\ ^{12}\text{N} &\rightarrow ^{12}\text{C} + e^+ + \nu_e, \end{aligned}$$

Neutral-current capture

$$\begin{aligned} \nu_e + ^{12}\text{C} &\rightarrow ^{12}\text{C}^* + \nu_e', & E_{th} &= 15.11 \text{ MeV}, \\ \nu_\mu + ^{12}\text{C} &\rightarrow ^{12}\text{C}^* + \nu_\mu', & E_{th} &= 15.11 \text{ MeV}, \\ \bar{\nu}_\mu + ^{12}\text{C} &\rightarrow ^{12}\text{C}^* + \bar{\nu}_\mu', & E_{th} &= 15.11 \text{ MeV}, \\ ^{12}\text{C}^* &\rightarrow ^{12}\text{C} + \gamma. \end{aligned}$$

The effective cross sections of the two reactions, the neutrino-electron reactions [36, 37] and neutrino-carbon reactions [38, 39], are given in Fig. 3.

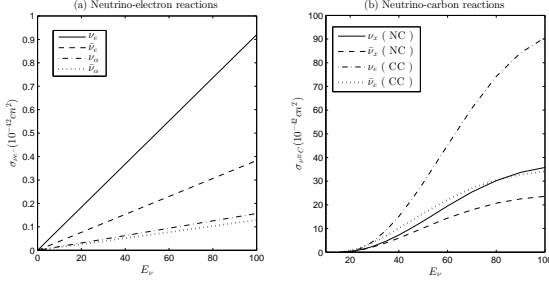


Fig. 3. The effective cross sections as functions of the neutrino energy. (a) the neutrino-electron reactions; (b) the neutrino-carbon reactions. $\alpha = \mu, \tau$, $x = e, \mu, \tau$.

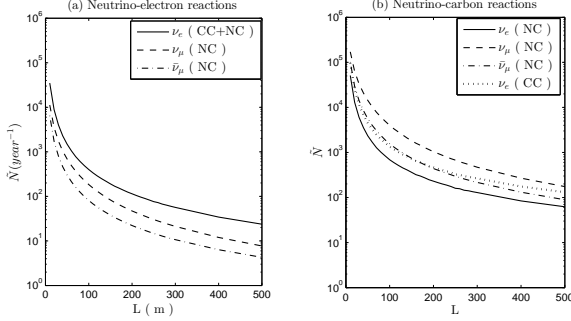


Fig. 4. The event numbers per year of accelerator neutrinos observed through various reaction channels as functions of the distance L . (a) the neutrino-electron reactions; (b) the neutrino-carbon reactions.

By using Eqs. (3) and (5), the neutrino event numbers per year were calculated. Fig. 4 shows the neutrino event numbers per year observed through two reaction channels changing with the distance L . It can be found that:

(i) The event numbers per year of different flavor neutrinos all decrease with the distance L for both the neutrino-electron reactions and neutrino-carbon reactions;

(ii) The total event number of accelerator neutrinos observed through the channel of the neutrino-carbon reactions is much larger than that of the neutrino-electron reactions;

(iii) For the neutrino-electron reactions, $\tilde{N}_{\nu_e}(CC + NC) > \tilde{N}_{\nu_\mu}(NC) > \tilde{N}_{\nu_\tau}(NC)$;

(iv) For the neutrino-carbon reactions, $\tilde{N}_{\nu_\mu}(NC) > \tilde{N}_{\nu_e}(NC) > \tilde{N}_{\nu_\tau}(NC)$; $\tilde{N}_{\nu_\mu}(NC)$ and $\tilde{N}_{\nu_e}(CC + NC)$ are both larger than $\tilde{N}_{\nu_\mu}(NC)$.

In the future, if the distance L , the detector efficiency, and the beam-on efficiency will be defined, the neutrino event numbers per year observed through various reaction channels can be calculated accurately. For example, $L = 60$ m, the detector efficiency and beam-on efficiency are both 50%, then the accurate neutrino event numbers per year can be given in Table 4. It is clear that there are a large number of accelerator neutrinos which can be used for observing sterile neutrino oscillations and measuring neutrino cross sections.

Table 4. Neutrino event numbers per year observed through various reaction channels while $L = 60$ m, the detector efficiency and beam-on efficiency are both 50%.

Reaction	$\tilde{N}_{\nu_e}(CC) + \tilde{N}_{\nu_e}(NC)$	$\tilde{N}_{\nu_\mu}(NC)$	$\tilde{N}_{\nu_\tau}(NC)$
νe^-	263	123	54
$\nu^{12}C$	824 + 426	2580	1005

4 Summary and Discussion

In this paper, the accelerator neutrino beam was studied in detail. With the code FLUKA, the processes of accelerator neutrino production at CSNS during the proton beam hitting on the tungsten target were simulated, and the yield efficiency, numerical flux, average energy of different flavor neutrinos were obtained. It concludes that three kinds of accelerator neutrinos have the same yield efficiency which is about 0.17 per proton. Therefore, they have the same yield event number per year which is 0.21×10^{22} for CSNS-I and 1.05×10^{22} for CSNS-II.

The detection of accelerator neutrinos through two reaction channels, the neutrino-electron reactions and neutrino-carbon reactions, was studied, and the neutrino event numbers were calculated. It can be found that the total event number of accelerator neutrinos observed through the channel of the neutrino-carbon reactions is much larger than that of the neutrino-electron reactions.

In our calculation, the detector efficiency and beam-on efficiency were hardly considered. In the future, until the completion of the design of neutrino detector at CSNS, the detector efficiency and beam-on efficiency will be given. Then, the detector errors will need to be reduced during the calculation of the neutrino event numbers. Furthermore, the statistical errors and systematic errors on the neutrino fluxes and cross sections also need to be considered for the design of neutrino experiment.

The author would like to thank X.-H. Guo, B.-L. Young, S. Wang and other CSNS colleagues for helpful discussions.

References

- 1 Boardman B. Spallation Neutron Source: Description of Accelerator and Target. RL-82-006, 1982
- 2 J-PARC TDR. Accelerator Technical Design Report for High-intensity Proton Accelerator Facility Project. JAERI-Tech2003-044, 2003
- 3 SNS Project Team. Spallation Neutron Source Design Manual. June, 1998
- 4 CSNS Project Team. China Spallation Neutron Source Feasibility Reaearch Report. Institute of High Energy Physics and Institute of Physics, Chinese Academy of Sciences, 2009 (in Chinese)
- 5 ESS Central Project Team. ESS Technical Design Report. ESS-doc-274-v15, 2015
- 6 Wei J. *Rev. Mod. Phys.*, 2003, **75**: 1383-1432
- 7 Wei J, Abell D T, Beebe-Wang et al. *Phys. Rev. ST Accel. Beams*, 2000, **3**: 080101
- 8 Athanassopoulos C, Auerbach L B, Bauer D et al. *Nucl. Instrum. Methods Phys. Res. A*, 1997, **388**: 149-172
- 9 Zeitnitz B. *Prog. Part. Nucl. Phys.*, 1985, **13**: 445-478
- 10 Zeitnitz B. *Prog. Part. Nucl. Phys.*, 1994, **32**: 351-373
- 11 Shirakata M J, Fujimori H, Irie Y et al. *Phys. Rev. ST Accel. Beams*, 2008, **11**: 064201
- 12 Saha P K, Shobuda Y, Hotchi H et al. *Phys. Rev. ST Accel. Beams*, 2009, **12**: 040403
- 13 SNS Project Team. Spallation Neutron Source Accumulator Ring and Transport Design Manual. June, 2003
- 14 VanDalen G J. Oscillations and Cross Sections at the SNS with a Large Cerenkov Detector. arXiv: 0309014 [nucl-ex]
- 15 Wang S, Fang S X, Fu S N et al. *Chin. Phys. C*, 2009, **33**: 1-3
- 16 Huang M Y, Wang S, Qiu J et al. *Chin. Phys. C*, 2013, **37**: 067001
- 17 Baussan E, Blennow M, Bogomilov M et al. *Nucl. Phys. B*, 2014, **885**: 127-149
- 18 Wei J, Fu S N, Tang J Y et al. *Chin. Phys. C*, 2009, **33**: 1033-1042
- 19 Kopp S E. *Phys. Rep.*, 2007, **439**: 101-159
- 20 Burman R L, Louis W C. *J. Phys. G: Nucl. Part. Phys.*, 2003, **29**: 2499-2512
- 21 Drexlin G, Eberhard V, Gemmeke et al. *Nucl. Instrum. Methods Phys. Res. A*, 1990, **289**: 490-495
- 22 Burman R L, Dodd A C, Plischke P. *Nucl. Instrum. Methods Phys. Res. A*, 1996, **368**: 416-424
- 23 Abe K, Abgrall N, Aihara H et al. *Nucl. Instrum. Methods Phys. Res. A*, 2011, **659**: 106-135
- 24 Aguilar-Arevalo A A, Anderson C E, Bartoszek L M et al. *Nucl. Instrum. Methods Phys. Res. A*, 2009, **599**: 28-46
- 25 Bonesini M, Guglielmi A. *Phys. Rep.*, 2006, **433**: 65-126
- 26 Bulanov S V, Esirkepov T, Migliozzi P et al. *Nucl. Instrum. Methods Phys. Res. A*, 2005, **540**: 25-41
- 27 Lazauskas R, Volpe C. *J. Phys. G: Nucl. Part. Phys.*, 2010, **37**: 125101
- 28 Louis W C. *Prog. Part. Nucl. Phys.*, 2009, **63**: 51-73
- 29 Aguilar-Arevalo A A, Bazarko A O, Brice S J et al. *Phys. Rev. Lett.*, 2007, **98**: 231801
- 30 Gervy G T, Green A, Green C et al. *Phys. Rev. D*, 2005, **72**: 092001
- 31 Ferrari A, Sala P R, Fasso A et al. *Fluka: Multi-Particle Transport Code*. CERN-2005-010, 2011
- 32 Vergados J D, Avignone III F T, Giomataris I. *Phys. Rev. D*, 2009, **79**: 113001
- 33 Dore U, Orestano D. *Rep. Prog. Phys.*, 2008, **71**: 106201
- 34 Gapozzi F, Fogli G L, Lisi E et al. *Phys. Rev. D*, 2014, **89**: 093018
- 35 Elnimr M, Stancu I, Yeh M et al. *The OscSNS White Paper*. arXiv:1307.7097 [physics.ins-det]
- 36 Arafune J, Fukugita M. *Phys. Rev. Lett.*, 1987, **59**: 367-369
- 37 Cadonati L, Calaprice F P, Chen M C. *Astropart. Phys.*, 2002, **16**: 361-372
- 38 Fukugita M, Kohyama Y, Kubodera K. *Phys Lett. B*, 1988, **212**: 139-144
- 39 Kolbe E, Langanke K, Vogel P. *Nucl. Phys. A*, 1999, **652**: 91-100